Physicochem. Probl. Miner. Process., 55(3), 2019, 802-811

http://www.journalssystem.com/ppmp

Physicochemical Problems of Mineral Processing

ISSN 1643-1049

Received January 30; reviewed; accepted February 25

The effect of pellet technology on direct reduction of jarosite residues from zinc hydrometallurgy

Yayun Wang [1], Huifen Yang [1], Xiaoqiang Hou [2], Wenjie Gao [2], Haiping Gui [2], Qian Liu [2]

[1] School of Civil and Resource Engineering, University of Science and Technology Beijing, Beijing, 100083, China
[2] Hanzhong Zinc Industry Co., Ltd, Shaanxi, 724200, China

Corresponding author: yanghf@ustb.edu.cn (Huifen Yang)

Abstract: In this study, the coal-based direct reduction technique has been applied to recover the valuable metals lead, zinc and ions from powdery and pellet jarosites. The influence of coal dosage of powdery and pellet jarosite separately on the volatilization rates of lead and zinc and on the metallization rate of iron was investigated. Results showed that the lead and zinc in both powdery and pellet jarosite could be effectively reduced with the volatilization rates higher than 95% and 99%, respectively. However, the iron reduction efficiency of pellet jarosite is better than that of powdery jarosite. The concentration of CO and CO_2 gas produced in the reduction process of two types of jarosite were detected and compared to investigate the difference of reduction mechanism between powdery and pellet jarosite. The result showed that the utilization of both CO and C during the reduction of pellet jarosite was higher than that of powdery jarosite. The theoretical analysis was carried out by gas analysis and scanning electron microscopy and energy dispersive spectrometer (SEM-EDS).

Keywords: jarosite residues, direct reduction, powdery jarosite, pellet jarosite, gas concentration analysis

1. Introduction

Jarosite residues are solid waste discharged during the zinc hydrometallurgy process, which were considered as the hazardous industrial waste due to the fine granularity, high water content, strong acidity, high content of heavy metal ions and poor stability (Calla-Choque et al., 2016; Montanaro et al., 2001; Pappu and Asolekar, 2006). At present, the annual accumulation of jarosite residues in China exceeds one million tons (Ju et al., 2011). The traditional treatment of metallurgical plant is generally stockpiling. However, this method severely threatens the environment and human health as it increases the exposure of heavy metals (Erdem and Özverdi, 2011; Özverdİ and Erdem, 2010; Salinas et al., 2001). Therefore, new strategies to treat jarosite residues or reclamation heavy metal resources in it via an environmentally- friendly manner is an imperative task.

Currently, the comprehensive utilization and resource recovery of jarosite residues are mainly focused on the preparation of building materials (Asokan et al. 2006; Asokan et al., 2010; Pappu et al., 2006; Mehra et al., 2016A, 2016B; Mymrin et al., 2005) and recovery of the valuable metals such as Cd, Zn, Ag, Cu and Pb (Chen et al., 2009; Hu et al., 2014; Malenga et al., 2015; Wang et al., 2018). The wet method and the fire-wet combined method have been widely employed for recycling one or more non-ferrous metals from jarosite residues. However, both two strategies have limitations. The former consumes extensive chemicals; while, the fire method generally results in the release of a large amount of SO_2 gas. Furthermore, both two methods mainly focus on the recovery of non-ferrous metals from jarosite but ignore the recovery of iron.

Considerable researches have been conducted to recover iron from solid wastes through direct reduction followed by magnetic separation (Guo et al., 2015; Yang et al., 2011; Yu et al., 2014). According to the characteristics of jarosite residues, adding CaO direct reduction roasting is a more feasible

DOI: 10.5277/ppmp19017

method. Through the direct reduction process, the compounds containing lead and zinc in the jarosite residues are reduced to the metallic lead and zinc, so that they can be separated and recovered (Wang et al., 2017). The compounds containing iron and sulfur in the jarosite residues are reduced to the metallic iron and CaS. In the following step, the metallic iron is recovered in the reduction product by grinding-magnetic separation. The harmful elemental sulfur is fixed in the reduction product.
In this study, two schemes are proposed, powdery jarosite and pellet jarosite were direct reduced to recover value metals lead, zinc and iron from jarosite residues. The reduction mechanism of two types of jarosite was investigated by gas analysis and SEM-EDS analysis.

2. Materials and methods

2.1. Materials

The jarosite residues sample used in this study was obtained from Shaanxi province, China. Its main chemical composition is shown in Table 1. The X-ray powder diffraction (XRD) analysis of the jarosite residues sample showed that iron mainly existed in the form of ammonium jarosite ($NH_4Fe_3(SO_4)_2(OH)_6$), plumbojarosite ($Pb(Fe_3(SO_4)_2(OH)_6)_2$) and franklinite ($ZnFe_2O_4$), lead in the form of plumbojarosite, and zinc in the form of franklinite, as shown in Fig. 1.

Table 1. Main chemical composition of jarosite residues

Constituents	Fe	Zn	Pb	S	Al_2O_3	SiO_2	MgO	CaO	loss on ignition
Content (wt%)	26.76	6.95	3.01	10.16	1.78	4.74	0.50	1.83	41.40

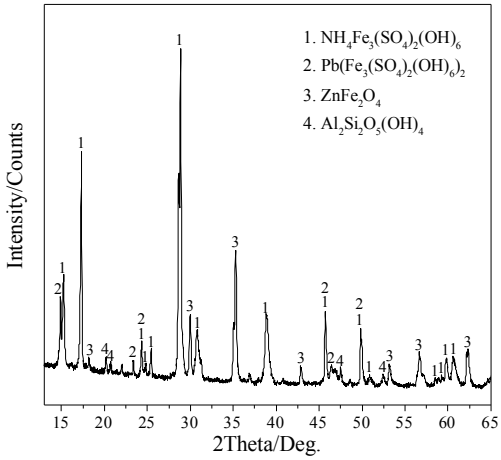

Fig. 1 XRD patterns of jarosite residues

A bituminous coal sample was used as reducing agent and it contained 4.56 wt% moisture, 17.36 wt% ash, 28.88 wt% volatiles, 49.20 wt% fixed carbon. In order to fix sulfur in the reduction product rather than volatilize into air, analytical grade CaO was added.

2.2. Experimental methods

The powdery jarosite are the mixture of jarosite residues, coal and CaO mixing according to mass ratio of 100: 35: 30. To prepare the pellet jarosite, the jarosite residues, CaO, coal and water were well mixed in accordance with mass ratio of 100: 25: 27.5: 35, and then the mixture were pressed to pellet, that is pellet jarosite. The crucible containing powdery jarosite or pellet jarosite was put into the atmosphere furnace and held for a reduction temperature of 1200℃ for 120 min. The CO and CO_2 gas concentration were detected in the reduction roasting process, and the diagrammatic sketch of reaction gas analyzer is shown in Fig. 2. Then, the reduction product was cooled to room temperature and the contents of lead, zinc, total iron and metallized iron inside were analyzed by chemical method.

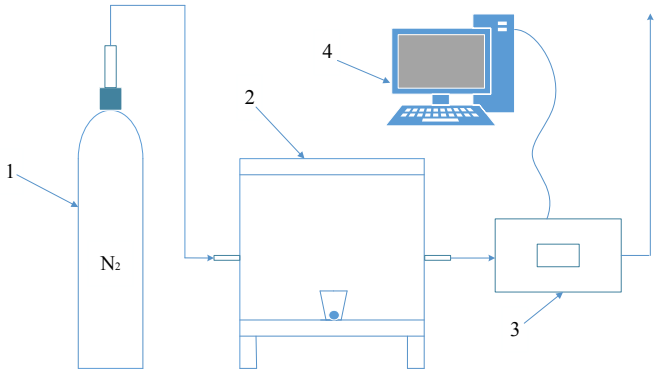

1. Nitrogen Bottle 2. Atmosphere Furnace
3. Gas Analyzer 4 . Computer

Fig. 2 Diagrammatic sketch of reaction gas analyzer

In this study, the recovery of lead and zinc during the reduction roasting was quantified by their volatilization rates. The volatilization rate of lead and zinc was calculated according to Equation (1); the iron metallization rate was calculated by Equation (2).

$$V=(1-\frac{C_2\times W_2}{C_1\times W_1})\times 100\% \quad (1)$$

$$M=\frac{C_M}{C_T}\times 100\% \quad (2)$$

where V is the volatilization rate of lead or zinc, C_1 and C_2 is the concentration of lead and zinc in jarosite and reduction product respectively, W_1 and W_2 is the weight of the jarosite and reduction product respectively, M is the iron metallization rate, C_M is the concentration of metallic iron and C_T is the concentration of total iron in the reduction product.

2.3. Analysis and characterization

The chemical analyses of jarosite and roasting product were measured by chemical titration in China University of Geosciences (Beijing) analysis laboratory. The CO and CO_2 gas concentration were detected by Germany MRU VARIO PLUS enhanced gas analyzer. The mineral and compositions of jarosite, reduction product and magnetic tailings were investigated by X-ray powder diffraction method (XRD) (Dmax-RD12kW) using Cu-K radiation at the scanning rate of 10 °/min from 10° to 90°. The microstructures of above products were also analyzed by scanning electron microscope (SEM) with energy dispersive spectrum (EDS) (Carl Zeiss EVO18), the sample for analysis was mounted in epoxy resin and polished.

3. Results and discussion

3.1. The effect of coal dosage on the direct reduction of jarosite

Fig.3 displays the effect of coal dosage on direct reduction of powdery jarosite at a reduction temperature of 1200℃ for 120 min. As shown in Fig. 3, with the increase of coal dosage from 20 to 40wt%, the coal dosage exhibited minor effect on the volatilization rates of lead and zinc, which were consistently greater than 97.03% and 99.53%, respectively. However, with the increase of coal dosage, the metallization rate of iron increased rapidly from 48.59% to 68.66%. When the coal dosage was greater than 35wt%, the metallization rate of iron remained almost constant. Therefore, the optimal coal dosage was selected as 35wt%.

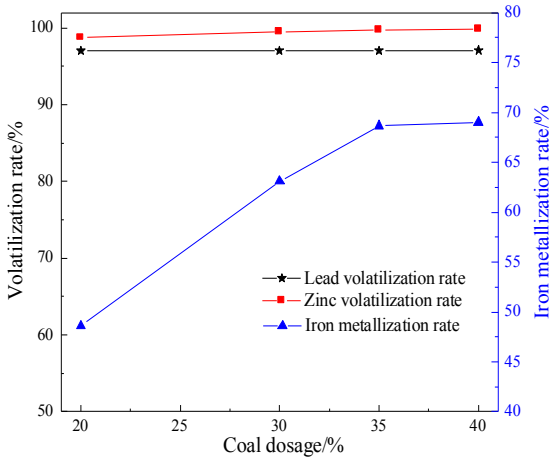

Fig. 3 The influence of coal dosage on direct reduction of powdery jarosite

Fig. 4 shows the effect of coal dosage on direct reduction of pellet jarosite at a reduction temperature of 1200℃ for 120 min.

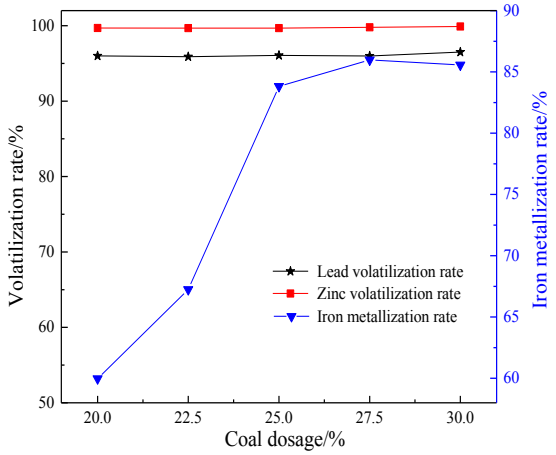

Fig. 4 The influence of coal dosage on the direct reduction of pellet jarosite

As shown in Fig. 4, within the coal dosage range from 20 to 30wt%, the quantity of coal had little influence on the volatilization rates of lead and zinc, which were consistently greater than 95.89% and 99.68%, respectively. However, a further increase on coal dosage led to a rapid increase of the metallization rate of iron from 59.97% to 83.82%. When the coal dosage was greater than 25wt%, the metallization rate of iron reached to constant. Therefore, the coal dosage with 25wt% was selected as the optimized condition for further experiment.

3.2. The CO and CO_2 gas concentration analysis

The concentration of CO and CO_2 gas produced during the reduction process was detected in order to analyze their effect on the reduction efficiency of jarosite residues. The rate of reduction (RDR) and the rate gasification (RCS) can be obtained by the oxygen balance and carbon balance, respectively (Chen et al., 2017; Jung, 2014, 2015; Kashiwaya et al., 2007). The formulas for the RDR and RCS are as follows:

$$\text{RDR (mol/min)}=\frac{\text{V}co(\%/\text{min})+2\times\text{V}co_2(\%/\text{min})}{\text{V}_{N_2}(\%/\text{min})}\times\text{V}_{N_2}(\text{L}/\text{min})\times\frac{1mol}{22.4L}$$

$$\text{RCS (mol/min)}=\frac{\text{V}co(\%/\text{min})+\text{V}co_2(\%/\text{min})}{\text{V}_{N_2}(\%/\text{min})}\times\text{V}_{N_2}(\text{L}/\text{min})\times\frac{1mol}{22.4L}$$

where Vco, V_{CO_2} and V_{N2} mean the real-time gas concentration, 22.4 means the gas molar volume.

Fig. 5 displays the CO and CO_2 gas concentration and the corresponding RDR, RCS in the reduction process of powdery jarosite.

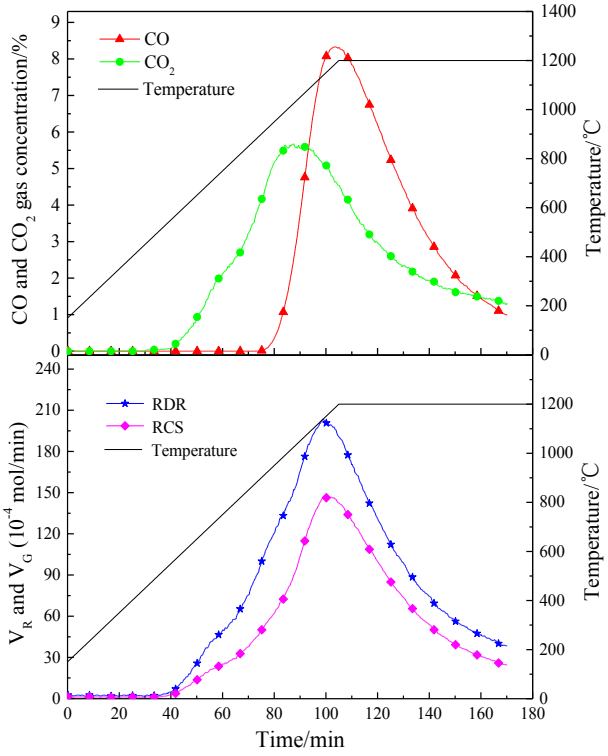

Fig. 5 The CO and CO_2 gas concentration and the corresponding RDR, RCS in the reduction process of powdery jarosite

As shown in Fig. 5, in the initial stage, the CO_2 gas concentration was almost zero; however, it exhibited a rapidly increase when the roasting time was longer than 40 min (550°C). With the increase of roasting time, the CO_2 gas concentration continued increasing until 85 min (1000°C). The variation of the CO gas concentration with time was similar to that of the CO_2 gas concentration. The CO gas was detected when the reduction time was longer than 75 min (900°C) and the concentration of CO reached at peak at 105 min (1200°C). The RDR and RCS gradually increased after 40 min reaction and decreased after reaching the maximum value in about 99 min. The variation on concentration of CO and CO_2 gas confirmed that, at the initial stage, the jarosite reduction should be initiated by the direct reduction of reaction (1), since the jarosite was in close contact with carbon. Afterward, CO started to be produced via reaction (2) and (3), and the CO was used for the jarosite reduction by reaction (4).

$$\text{Jarosite} + \text{C(s)} = \text{Reduced Jarosite} + \text{CO}_2\text{(g)} \quad (1)$$

$$\text{C(s)} + \text{CO}_2\text{(g)} = \text{CO(g)} \quad (2)$$

$$\text{Jarosite} + \text{C(s)} = \text{Reduced Jarosite} + \text{CO(g)} \quad (3)$$

$$\text{Jarosite} + \text{CO(g)} = \text{Reduced Jarosite} + \text{CO}_2\text{(g)}. \quad (4)$$

The CO and CO_2 gas concentration and the corresponding RDR, RCS in the reduction process of pellet jarosite were shown in Fig.6. As shown in Fig. 6, there was no CO_2 gas detected during the initial reaction stage; however, the concentration of CO_2 appeared a rapid increasing when the roasting time was longer than 40 min (550°C) and it reached to the maximum value at 75 min (900°C) and exhibited a rapid decrease during 75 to 125 min and a mild reduction after 125 min. The variation of the CO gas concentration with time was similar to the change of the CO_2 concentration with time. The CO gas concentration reached a maximum at 95 min (1100°C) and then rapidly decreased. The change on the concentration of CO and CO_2 gas in the system indicated that the jarosite was initially reduced by carbon to produce CO_2 via reaction (1). Hereafter, CO was generated via reaction (2) and (3), and the produced CO was used as reduction agents for the jarosite reduction via reaction (4). The RDR increased rapidly after 40 min reaction and the maximum value was achieved after 95 min. Different from other parameters, the RCS increased lowly from around 40 min and then decreased after reaching the maximum value in about 95 min. The highest RCS value did precisely match with the largest CO gas

concentration, which indicating that the pellet scheme improved the utilization of CO in the reduction of jarosite. Compared with relationship between the RCS and CO gas concentration of powdery jarosite, the pellet jarosite has higher CO utilization.

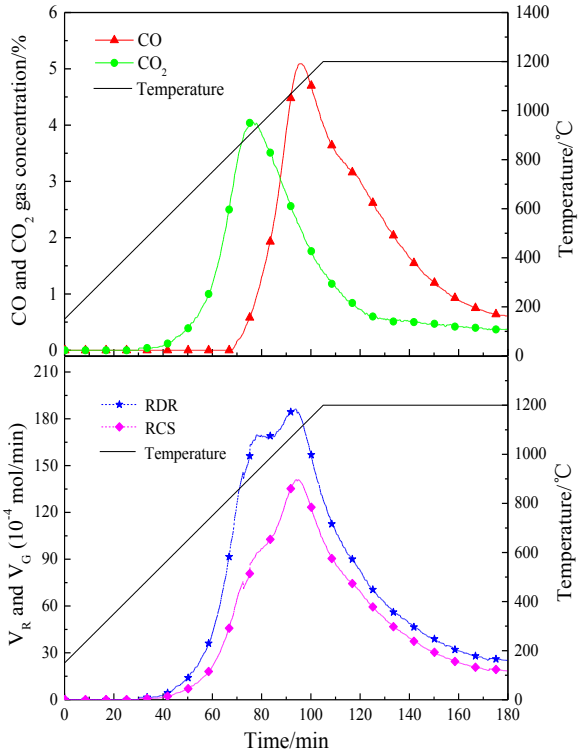

Fig. 6 The CO and CO_2 gas concentration and the corresponding RDR, RCS in the reduction process of pellet jarosite

In order to figure out the fixed carbon utilization, the ratio of RDR to RCS with time was analyzed since the ratio of RDR to RCS showed the efficiency of carbothermic reduction of jarosite with char. If the ratio is close to 1, indicating that the fixed carbon utilization rate is a relatively low value, which represents the overall reaction by the equation (3). On the other hand, if the ratio is close to 2, showing a higher fixed carbon utilization rate, which represents the overall reaction by the equation (1). This indicates that the generated CO was completely utilized in the reduction reaction (Jung, 2015; Kashiwaya et al., 2007; Katsioti et al., 2006). The ratio of RDR to RCS during the direct reduction of powdery jarosite and pellet jarosite was shown in Fig.7.

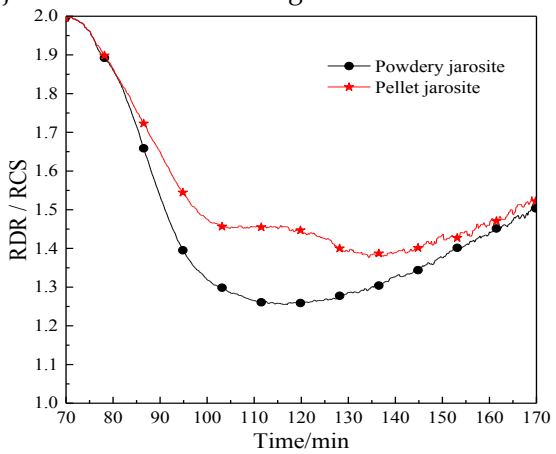

Fig. 7 The ratio of RDR to RCS during the direct reduction of powdery jarosite and pellet jarosite

As shown in Fig.7, the ratio of RDR to RCS was almost 2, which indicated that the jarosite was reduced by reaction (1). This is due to the close contact between jarosite and fixed carbon. At the initial stage, the jarosite is reduced by fixed carbon. With the reaction continues, the CO plays a predominate role in the reduction of jarosite via reaction (4). The Fig.7 show that the ratio of RDR to RCS of pellet jarosite was higher than that of powdery jarosite from 70 min to 170 min. This indicates that the pellet jarosite has higher fixed carbon utilization than powdery jarosite.

In summary, the utilization of CO and fixed carbon in pellet jarosite is higher than that of powdery jarosite. It inferred that the pellet of powdery jarosite plays a significant role in improving the utilization of CO and fixed carbon.

3.3. The chemical and phase composition analysis

The main chemical and phase composition of reduction products were shown in Table 2 and Fig.8 respectively. Only a small amount of lead and zinc are found in the reduced product, indicating that lead and zinc have been well reduced and volatilized. Fig.8 shows some diffraction peaks of Fe_3O_4 and $Ca_2Fe_2O_5$ still present in the reduced product of powdery jarosite, and the diffraction peaks of metallic iron in the reduction product of pellet jarosite is obviously stronger than that of powdery jarosite. It's well to know that the reduction effect of pellet jarosite is better than powdery jarosite. The results of chemical and phase composition analysis of reduction products can be nicely explained by the utilization of CO and fixed carbon in reduction process.

Table 2. Main chemical composition of reduction products/(wt%)

Constituents	Fe	Zn	Pb	S	Al_2O_3	SiO_2	MgO	CuO	CaO
powdery jarosite	33.80	0.02	0.11	7.81	3.48	11.95	2.69	1.75	36.87
pellet jarosite	38.33	0.01	0.13	14.40	2.75	8.79	2.12	1.51	30.96

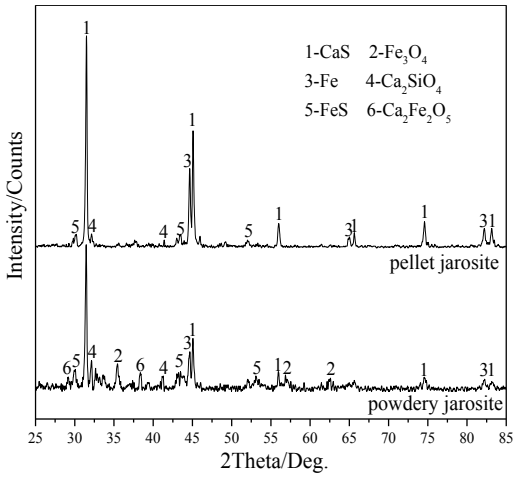

Fig. 8 XRD patterns of reduction products

3.4. The microstructure analysis

In order to compare the reduction efficiency of powdery jarosite and pellet jarosite, their reduction product was analyzed by scanning electron microscope coupled with energy dispersive spectrometer (SEM-EDS). The SEM-EDS images of reduction product of powdery jarosite are shown in Fig. 9.

Fig. 9 shows that different color regions were found in the reduction products of powdery jarosite after direct reduction. The representative areas B and C were respectively analyzed. The B regions are mainly bright white and gray parts. And according to EDS analysis, the main elements in bright white point 1 are Fe, O and S. Thus, the bright white areas in B regions might consist of a mixture of metallic iron, iron oxides and iron sulfides. The main elements in gray point 2 are Si, Ca, Mg, Al and O, and the gray areas in B regions might be various silicates. The C regions also were mainly bright white and gray portion. However, a large number of small particles were found in the C regions. The EDS analysis

showed that the main element in bright white point 3 was Fe, and the bright white areas in C regions were pure iron particles. The main elements in gray point 4 are Si, Ca, Fe, Al and O, and the gray areas in C regions may be the silicates. The Fig.8 indicates that the iron reduction from powdery jarosite was not satisfied.

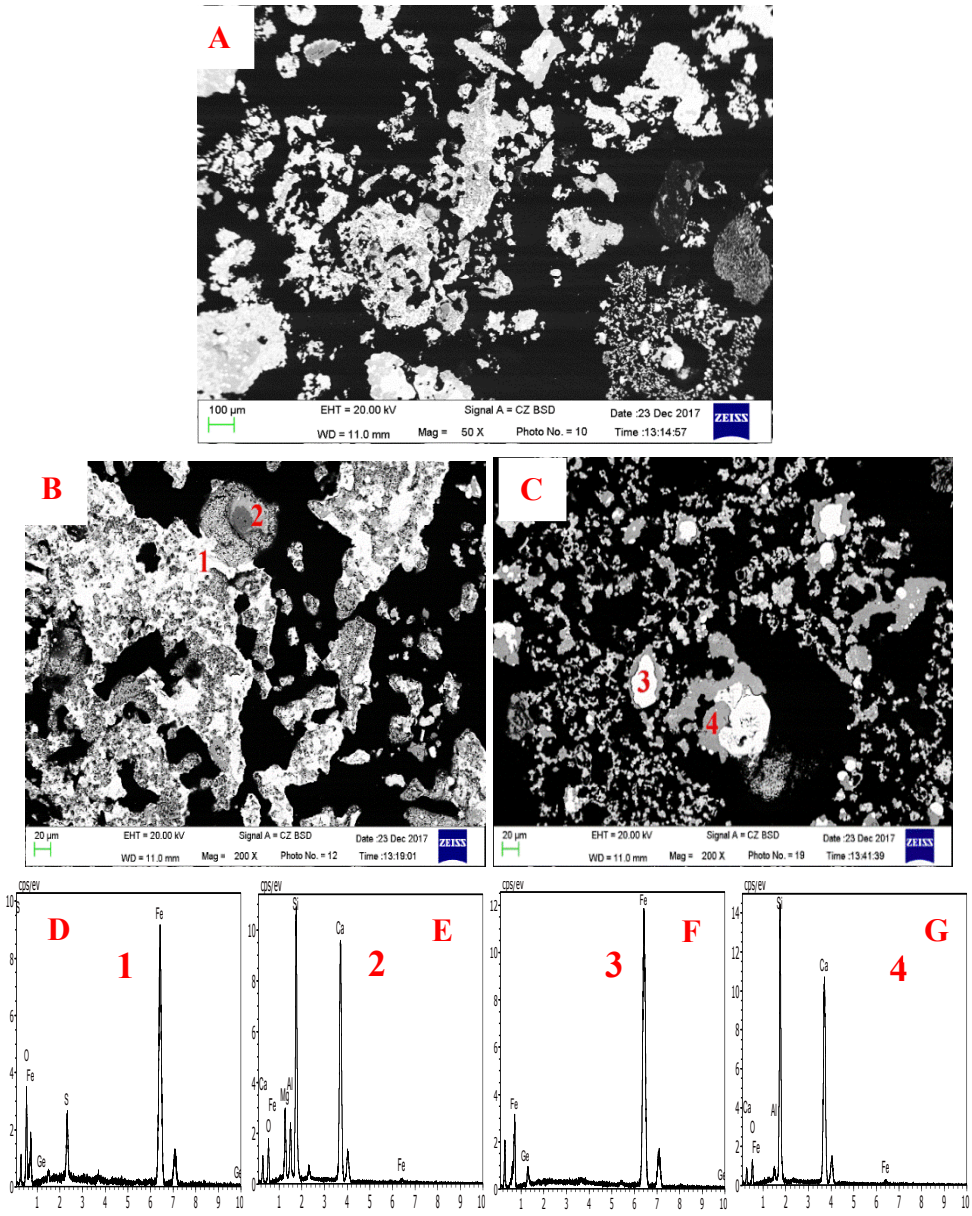

Fig. 9. SEM images of reduction product of powdery jarosite (A, B, C) and corresponding EDS at Point 1 (D); Point 2 (E); Point 3 (F); Point 4 (G)

Fig.10 displays the SEM-EDS images of reduction product of pellet jarosite. As shown in Fig.10, the bright white and gray are the main areas of reduction product of pellet jarosite, there are also some black and light white silky areas in the reduction product. Comparing Fig. 8, it can be seen that Fig. 10 has more bright white metallic iron areas. At the same time, almost no iron oxide regions were found in Fig. 10, indicating that the pellet jarosite has a better iron reduction efficiency. Lead and zinc were not detected in Figures 9 and 10, indicating that lead and zinc have been well reduced and recovered. The size of metallic iron particles in pellet jarosite reduction product is relatively uniform, its particle size is generally about 20 µm, it is conducive to the recovery of metallic iron by grinding and magnetic separation.

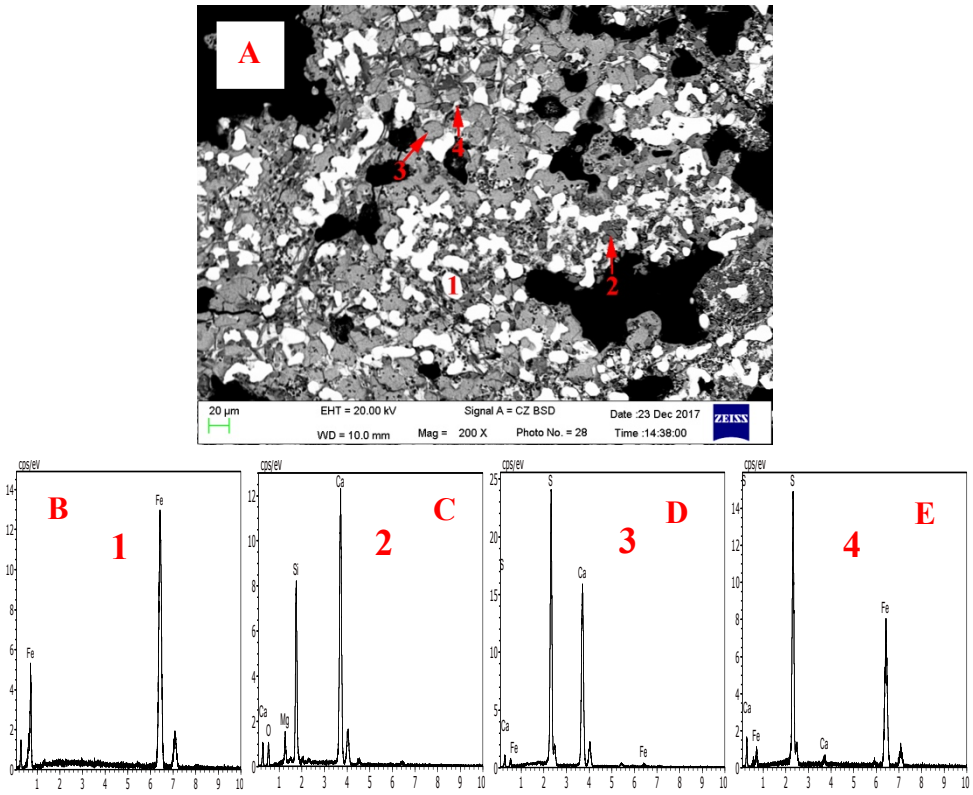

Fig. 10 SEM images of reduction product of pellet jarosite (A) and corresponding EDS at Point 1 (B); Point 2 (C); Point 3 (D); Point 4 (E)

4. Conclusions

According to the study, the following conclusions can be drawn.

(1) In this study, the coal-based direct reduction technique has been applied to recover the valuable metals lead, zinc and ions from powdery and pellet jarosites.

(2) The volatilization rates of lead and zinc are 97.07% and 99.75%, respectively, the iron metallization rate is 68.66%, when the powdery jarosite with the coal dosage of 35% was roasted at reduction temperature of 1200℃ for 120 min. Under the same condition with the coal dosage of 25%, the volatilization rates of lead and zinc are 95.99% and 99.78%, the iron metallization rate is 85.98% of pellet jarosite.

(3) The iron reduction effect of pellet jarosite is superior to that of powdery jarosite. Compared with the powdery jarosite, the pellet jarosite improved the utilization of CO and C in the reduction process, which was conducive to the iron reduction.

(4) The results show that pellet process is more suitable for recovering valuable metals from jarosite residues through direct reduction. This method enables the comprehensive utilization of valuable metals from hazardous jarosite residues.

References

ASOKAN, P., SAXENA, M., ASOLEKAR, S. 2010. *Recycling hazardous jarosite waste using coal combustion residues*. Materials Characterization. 61, 1342-1355.

ASOKAN, P., SAXENA, M., ASOLEKAR, S. R. 2006. *Hazardous jarosite use in developing non-hazardous product for engineering application*. Journal of Hazardous Materials. 137, 1589-1599.

CALLA-CHOQUE, D., NAVA-ALONSO, F., FUENTES-ACEITUNO, J. 2016. *Acid decomposition and thiourea leaching of silver from hazardous jarosite residues: Effect of some cations on the stability of the thiourea system*. Journal of Hazardous Materials. 317, 440-448.

CHEN, C., SUN, T., WANG, X., HU, T. 2017. *Effects of MgO on the Reduction of Vanadium Titanomagnetite Concentrates with Char*. JOM. 69, 1759-1766.

CHEN, Y., TANG, M., YANG, S., HE, J., TANG, C., YANG, J., LU, J. 2009. *Novel technique of decomposition of ammonium jarosite bearing indium in NaOH medium*. The Chinese Journal of Nonferrous Metals. 19, 1322-1331.

ERDEM, M., ÖZVERDI, A. 2011. *Environmental risk assessment and stabilization/ solidification of zinc extraction residue: II. Stabilization/solidification*. Hydrometallurgy. 105, 270-276.

GUO, D., HU, M., PU, C., XIAO, B., HU, Z., LIU, S., ZHU, X. 2015. *Kinetics and mechanisms of direct reduction of iron ore-biomass composite pellets with hydrogen gas*. international journal of hydrogen energy. 40, 4733-4740.

HU, H., DENG, Q., LI, C., XIE, Y., DONG, Z., ZHANG, W. 2014. *The recovery of Zn and Pb and the manufacture of lightweight bricks from zinc smelting slag and clay*. Journal of Hazardous Materials. 271, 220-227.

JU, S., ZHANG, Y., ZHANG, Y., XUE, P., WANG, Y. 2011. *Clean hydrometallurgical route to recover zinc, silver, lead, copper, cadmium and iron from hazardous jarosite residues produced during zinc hydrometallurgy*. Journal of Hazardous Materials. 192, 554-558.

JUNG, S. M. 2014. *Thermogravimetry and Reaction Gas Analysis of the Carbothermic Reduction of Titanomagnetite Ores with Char*. ISIJ International, 54, 781-790.

JUNG, S. M. 2015. *Effects of $CaO/CaCO_3$ on the Carbothermic Reduction of Titanomagnetite Ores*. Metallurgical & Materials Transactions B. 46, 1162-1174.

KASHIWAYA, Y., KANBE, M., ISHII, K. 2007. *Reaction Behavior of Facing Pair Between Hematite and Graphite: A Coupling Phenomenon of Reduction and Gasification*. ISIJ International. 41, 818-826.

KATSIOTI, M., TSAKIRIDIS, P., LEONARDOU-AGATZINI, S., OUSTADAKIS, P. 2006. *Examination of the jarosite–alunite precipitate addition in the raw meal for the production of sulfoaluminate cement clinker*. Journal of Hazardous Materials. 131, 187-194.

MALENGA, E. N., MULABA-BAFUBIANDI, A., NHETA, W. 2015. *Alkaline leaching of nickel bearing ammonium jarosite precipitate using KOH, NaOH and NH_4OH in the presence of EDTA and Na_2S*. Hydrometallurgy. 155, 69-78.

MEHRA, P., GUPTA, R. C., THOMAS, B. S. 2016A. *Assessment of durability characteristics of cement concrete containing jarosite*. Journal of Cleaner Production. 119, 59-65.

MHERA, P., GUPTA, R. C., THOMAS, B. S. 2016B. *Properties of concrete containing jarosite as a partial substitute for fine aggregate*. Journal of Cleaner Production. 120, 241-248.

MONTANARO, L., BIANCHINI, N., RINCON, J. M., ROMERO, M. 2001. *Sintering behaviour of pressed red mud wastes from zinc hydrometallurgy*. Ceramics international. 27, 29-37.

MYMRIN, V. A., PONTE, H. A., IMPINNISI, P. 2005. *Potential application of acid jarosite wastes as the main component of construction materials*. Construction and building materials. 19, 141-146.

ÖZVERDI A., ERDEM, M. 2010. *Environmental risk assessment and stabilization/ solidification of zinc extraction residue: I. Environmental risk assessment*. Hydrometallurgy. 100, 103-109.

PAPPU, A., SAXENA, M., ASOLEKAR, S. R. 2006. *Jarosite characteristics and its utilisation potentials*. Science of the total environment. 359, 232-243.

SALINAS, E., ROCA, A., CRUELLS, M., PATINO, F., CORDOBA, D. 2001. *Characterization and alkaline decomposition–cyanidation kinetics of industrial ammonium jarosite in NaOH media*. Hydrometallurgy. 60, 237-246.

WANG, C., LI, K., YANG, H., LI, C. 2017. *Probing Study on Separating Pb, Zn, and Fe from Lead Slag by Coal-based Direct Reduction*. ISIJ International. 57, 996-1003.

WANG, Y., YANG, H., JIANG, B., SONG, R., ZHANG, W. 2018. *Comprehensive recovery of lead, zinc, and iron from hazardous jarosite residues using direct reduction followed by magnetic separation*. International Journal of Minerals, Metallurgy, and Materials. 25, 123-130.

YANG, H., JING, L., ZHANG, B. 2011. *Recovery of iron from vanadium tailings with coal-based direct reduction followed by magnetic separation*. Journal of Hazardous Materials. 185, 1405-1411.

YU, W., SUN, T., LIU, Z., KOU, J., XU, C. 2014. *Effects of particle sizes of iron ore and coal on the strength and reduction of high phosphorus oolitic hematite-coal composite briquettes*. ISIJ International. 54, 56-62.